Sustainable Defluoridation of Water: Fixed-Bed Adsorption Column Studies Using Zirconium Doped Sunflower Seed Husk as an Adsorbent

Bhavya N.S.[1], H.V. Jayaprakash[2*], H.S. Lalithamba[3], Poornima G. Hiremath[4], Suresh Kumar H.M.[5], Prashanth G.K.[6]

[1]Sri Siddhartha Institute of Technology, Maraluru, Tumkuru, Sri Siddhartha Academy of Higher Education, Agalkote, Tumkur-572107, Karnataka, India: bhavyarenu87@gmail.com
[2]Associate Professor, Department of Chemistry, Sri Siddhartha Institute of Technology, Maraluru, Tumkur-572105, Karnataka, India: jpvpsb@gmail.com*
[3]Professor and Head, Department of Chemistry, Siddaganga Institute of Technology, B.H. Road, Tumkur-572103, Karnataka, India: hsl@sit.ac.in
[4]Associate Professor, Department of Chemical Engineering, Siddaganga Institute of Technology, B.H. Road, Tumkur-572103, Karnataka, India: pgh@sit.ac.in
[5]Professor, Department of Physics, Siddaganga Institute of Technology, B.H. Road, Tumkur-572103, Karnataka, India: hms@sit.ac.in
[6]Associate Professor, Department of Chemistry, Sir M. Visvesvaraya Institute of Technology, Bengaluru-562157, Karnataka, India: prashanth_chem@sirmvit.edu
**Corresponding Author: jpvpsb@gmail.com, Sri Siddhartha Institute of Technology, Maraluru, Tumkuru, Sri Siddhartha Academy of Higher Education, Agalkote, Tumkur-572107, Karnataka, India, Telephone Number: 08162200314.*

KEYWORDS

Adsorption, defluoridation, adsorbent, zirconium, sunflower seed husk, column studies.

ABSTRACT

Numerous health problems resulting from elevated fluoride levels in drinking water affect millions of people worldwide. In order to eliminate ions of fluoride from water, the current study details the adsorption effectiveness of a zirconium-doped sunflower seed husk (ZrO_2/SSH) adsorbent made using a hydrothermal carbonization process. Fourier transform infrared spectroscopy (FTIR), X-ray diffraction (XRD), transmission electron microscopy (TEM), and scanning electron microscopy (SEM) were utilized to evaluate the powdered adsorbent., In a bed that is fixed, the potential of zirconium-doped sunflower seed husk to remove fluoride from real and synthetic groundwater samples was investigated. Fluoride removal was examined in relation to key parameters like input flow rate, height of the column bed, and influent fluoride content of solution. To assess the experimental data and comprehend the impact on biosorption performance, Yoon-Nelson and Thomas models were employed. Fluoride ion desorption was achieved by pumping a 0.1 M HCl solution. Through multiple cycles of fluoride adsorption and desorption, the reusability of the adsorbent was investigated. The effectiveness of ZrO_2/SSH adsorbent in removing fluoride from groundwater samples in the Tumakuru district's Pavagada taluk was investigated in a packed column. According to the results of the entire investigation, this adsorbent showed promise in removing fluoride from groundwater and aqueous solutions.

1. INTRODUCTION

Heavy metals have been extracted from aqueous solutions using a variety of analytical techniques. Adsorption is a technique that many researchers have found to be very selective, effective, simple

to use, and economical (Reddy, Lakshmipathy and Sarada. 2014). Because activated carbon is so expensive, researchers are using inexpensive biomass as adsorbents to remove fluoride from water. For the elimination of fluoride, there must be alternative adsorbents that are as effective but less expensive, and they were discovered to be promising (Asuquo, Martin and Nzerem. 2018). In general, agricultural residues and garbage are inexpensive, plentiful, renewable, largely non-toxic, and environmentally kind (Jain, Garg and Kadirvelu. 2009). According to the circular bioeconomy and "green chemistry" theories, it is crucial to use and convert agricultural waste into goods with added value. An essential oil seed crop that is farmed all over the world, sunflower provides high-quality oil and dietary fiber, both of which are vital for human health (Feizi and Jalali, 2015). Because sunflower biomass contains lignin and functionalities that contain oxygen, like hydroxyl and carboxyl moieties, it has a wide range of chemical variability. The lignocellulosic waste material utilized in this study, sunflower seed shells (SSS), exemplifies an ideal, cost-effective adsorbent. Up to 30% of sunflower husks are produced by the oil industry, which also produces SSS. Sunflower seed shells, often regarded as waste byproducts of oil production, are typically burnt to produce heat. The local oil business in our study uses these shells to heat boilers (Saleh, El-Refaey and Mahmoud 2016).

The sorption process can be performed using column methods, making it important to test the sorption ability of SSH as an alternative adsorbent in both systems. Zirconium (IV) oxychloride octahydrate ($ZrOCl_2$.$8H_2O$) doped sunflower seed husk have not been previously tested for treating fluoride-contaminated water. When zirconium is found in its oxide state, also referred to as zirconia or zirconium oxide, it is a hard transition metal with countless uses. Oral toxicity is low for zirconium. This element is primarily found as insoluble dioxide in water with a normal pH and is biologically inactive. Aside from these characteristics, Zr(IV) exhibits a particular binding to the F^- ion via the Lewis acid-base interaction. Due to its strong affinity for fluoride ions, zirconium has been utilized as an adsorbent in a variety of ways for water treatment procedures (Wang *et al.* 2020). No specific guidelines have been established for zirconium levels in drinking water. The zirconium modified sunflower seed husk (ZrO_2/SSH) adsorbents, designed to remove fluoride from aqueous solutions, are safe for human health. The column studies were performed to explore the fluoride removal efficiency of zirconium-doped adsorbent under varying rates of flow, starting concentrations of fluoride, and heights of the bed. Numerical analysis was performed, and the experimental data were modeled using two approaches for both static and dynamic systems. Regeneration of the adsorbent was investigated in the column system combined with distilled water and 0.1 M HCl. The adsorbent was characterized prior to and following fluoride adsorption using FTIR, SEM, XRD and TEM techniques (Mani and Bhandari, 2022).

2. MATERIALS AND METHODS

2.1. Chemicals and reagents

The sunflower seeds were acquired from a nearby marketplace of Tumkur, Karnataka, India. The precursor used is Zirconium oxychloride octahydrate ($ZrOCl_2 \cdot 8H_2O$) were obtained from Veeresh Scientifics, Tumkur, Karnataka, India, which is analytical grade and utilized without further purification. Water that has been deionized was utilized throughout the experiment.

2.2. Pretreatment of sunflower seed husk

Sunflower seeds were separated from husk and after being regularly cleaned with distilled water to get rid of inorganic contaminants, the husk was filtered and dried in an oven set to 333 K for the entire night to lower its moisture content. The dry SSS was then crushed and sieved to produce particles with a size of # 0.3 mm.The powder obtained was stored for further analysis.

2.3. Preparation of Biochar (Adsorbent)

In a magnetic stirrer, 5 g of sunflower seed husk waste powder (SSH) was combined with 1 mol/L zirconium solution for two hours. The stirred product is kept in a 100 ml polytetrafluoroethylene (PTFE) inner steel autoclave (hydrothermal bomb) in an oven for 6 hours at 180 ^{o}C. The resultant solution is washed using deionised water and filtered using whattman filter paper 42 till the product's pH becomes neutral (7). The product is then calcined for 8 hours at 5 ^{o}C to obtain zirconium treated biochar (ZrO_2/BC). Zirconium-untreated biochar was just regular biochar.

2.4. Preparation of standard fluoride solution

1000 mL of purified water were used to dissolve 2.21 g of sodium fluoride to create a 1000 mg/L stock solution of fluoride. A fluoride electrode and an ion meter were used to measure the fluoride levels. To control the samples' ionic strength in relation to reference solutions, a 1:10 solution of total ionic strength adjusting buffer III (TISAB-III) was added. TISAB-III eliminated complexing ions' interfering effect, separated weakly bound fluoride ions, and maintained the solution's pH between 5 and 5.5 (Hiremath and Theodore, 2017).

2.5. Column adsorption experiments

Because column operations yield good results, are easy to use, inexpensive, and quickly scaled up from a laboratory procedure, they are crucial.

In this study, a fixed-bed adsorption column of 50 cm in height and 2 cm in internal diameter was used. The fluoride solution was circulated through the bed using a peristaltic pump at a steady inflow rate while the ZrO_2/SSH adsorbent was packed in the column. At regular periods, the wastewater was collected. An ion-selective electrode was used to monitor the effluent's fluoride content in order to calculate the breakthrough curve (Kovo *et al.* 2023; Bai *et al.* 2022). The experiments were conducted using varied initial fluoride solutions (10, 12, 14 mg/L), packed bed heights (5, 7, 9 cm), and flow rates (7, 8.5, and 10 ml/min). A fluoride ion selective electrode was used to measure the amount of fluoride that remained after the top of the packed column was periodically used to collect the effluent solution. When 99.5% of the initial effluent concentration was exceeded, the column's operation was terminated. The ratio of the C_t/C_o (where C_t and C_o represent the fluoride concentration of effluent and influent, respectively) was plotted against time to determine the column's breakthrough curve. The effluent concentration (C_t) reaching a specific percentage is known as the "breakthrough point" [e.g., 5% of the initial concentration (C_o)]. The point at which the initial concentration (C_o) and the effluent concentration (C_t) are almost equal is known as the exhaustion point. The area above the breakthrough curves is assessed following their charting (Aksu and Gönen, 2004).

The total quantity of fluoride adsorbed was determined by equation 1:

Q_{ad} = flow rate * Area above the curve (1)

The total fluoride content in the column is given by equation 2:

$Q_{total} = C_o * \text{Flow rate} * t_{exh}$ (2)

Where, C_o is the initial concentration of fluoride, t_{exh} represents the exhaustion time.

The overall fluoride elimination % was assessed using equation 3:

$\%\text{Fluoride removal} = Q_{ad}/Q_{total} * 100$ (3)

3. RESULT AND DISCUSSION

3.1. Characterization of the biosorbent

3.1.1. XRD Analysis

Fig.1 represents the XRD pattern of synthesized ZrO_2/SSH adsorbent. Prominent diffraction peaks were observed at 2θ = 30.42°, 34.93°, 38.01°, 50.58°, 60.06°, 63.38°, and 74.29°, corresponding to the (111), (200), (102), (220), (311), (222), and (400) planes, respectively. These planes were good agreement with JCPDS Card Nos. 42-1164 and 37-1484 (Shinde *et al.* 2018). The results indicate that ZrO_2 adsorbent exhibit both monoclinic and tetragonal phases (Annu, Sivasankari and Krupasankar. 2020, Al-Zaqri *et al. 2021*)..From the XRD pattern, it is evident that the (111) plane shows the highest intensity, suggesting significant crystalline growth along this plane. According to the Scherrer formula 4, the ZrO_2 adsorbent's average crystallite size was 29.4 nm (Muthuvel *et al*. 2020).

$$D = \frac{k\lambda}{\beta Cos\theta} \quad (4)$$

where D is the crystallite size, β-is the full width half maximum of the peak and λ- is the X-ray wavelength of CuKα radiation.

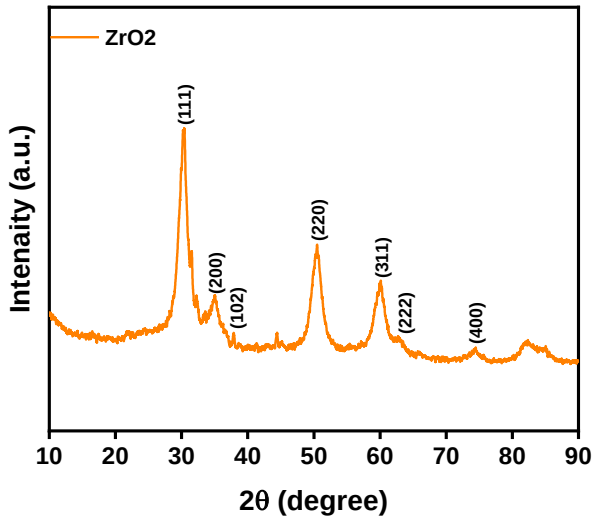

Fig. 1: XRD pattern of synthesized ZrO_2 NPs.

3.1.2. FT-IR analysis

The FTIR spectrum of ZrO_2/SSH adsorbent is resented in Fig.2. A wide band observed at 3415 cm^{-1}corresponds to the asymmetric stretching of OH groups from adsorbed moisture and

associated hydrogen bonds. Notable peaks were observed at 2956, 2856, 2060, 1590, 1356, 1046, and 769 cm^{-1}. Strong peaks at 2956 cm^{-1} and 2856 cm^{-1} were ascribed to stretching vibrations of the C–H bond. Medium-intensity peaks between 2060 cm^{-1} and 1590 cm^{-1} were related to C=O stretching of carboxyl groups, potentially indicating the presence of an amide group responsible for reducing Zr^{4+} ions to ZrO_2 adsorbent and C=C unsaturation in the plant seed extract. Stretching vibrations of C–C were represented by the band at 1356 cm^{-1}. At 1046 cm^{-1}, peaks were attributed to stretching vibrations of C–N of aliphatic amines (Goyal, *et al.* 2021). Additionally, a medium bending peak at 815 $cm^{-}1$ was ascribed to stretching vibrations between C and H. Finally, additionally, the characteristic bands at 769 and 510 $cm^{-1}$are indicatives of Zr–O–Zr bending vibrations, confirming the formation of the ZrO_2 structure (Suriyaraj, *et al* 2019).

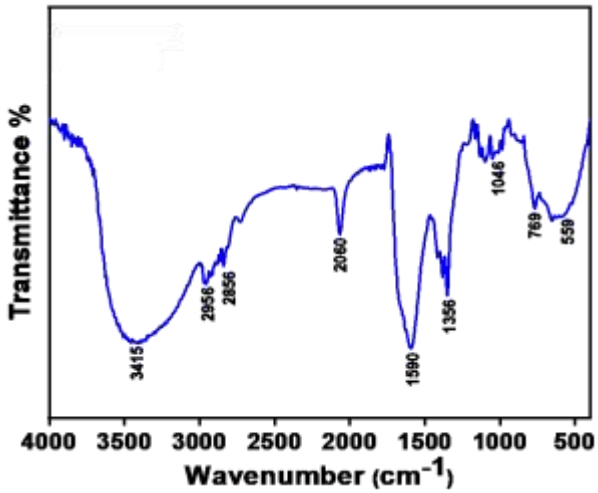

Fig. 2: FTIR spectra of synthesized ZrO_2 NPs.

3.1.3. SEM and EDX analysis

SEM and EDX analyses are effective techniques for examining the morphology and chemical composition of synthesized samples. The surface morphology of ZrO_2/SSH adsorbent at various magnifications is illustrated in Fig.3(a–c). The SEM images reveal that the ZrO_2 adsorbent exhibits a heterogeneous structure with agglomeration and irregularly formed clusters. The EDX spectrum of the ZrO_2 adsorbent, shown in Fig.3(d), confirms the synthetic nanoparticles' elemental composition, indicating the existence of zirconium (Zr) and oxygen (O). This analysis verifies the successful synthesis of ZrO_2 NPs.

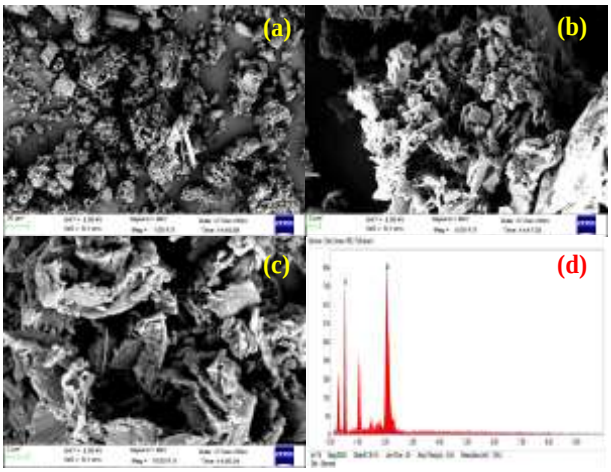

Fig. 3: (a-c) SEM images of synthesized ZrO_2 NPs at different magnification and (d) EDX spectra of ZrO_2 NPs

3.1.4. TEM analysis

Transmission electron microscopy (TEM) was employed to study the shape and crystallinity of the synthesized ZrO_2/SSH prepared via the green method. TEM and HRTEM micrographs of the ZrO_2 adsorbent are presented in Fig.4 (a-c). The TEM images as shown in Fig.4a and b reveal nanoparticles with hexagonaland irregular shapes. The high-resolution TEM (HRTEM) images seen in Fig.4c further show distinct lattice fringes with a d-spacing of 0.19 nm, which relates to the (220) plane, confirming good consistency with the XRD results. Furthermore, the pattern of the selected area electron diffraction (SAED) in Fig. 4d displays a series of irregular bright rings, indicating the polycrystalline structure of the synthesized nanoparticles. The SAED pattern reveals lattice fringes corresponding to the (111) and (002) planes, which agree well with the XRD information.

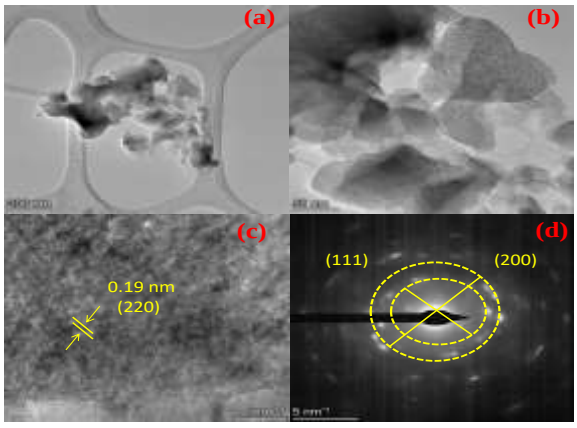

Fig. 4: TEM images of (a, b) ZrO_2 NPs, (c, d) HR-TEM and SEAD pattern ZrO_2 NPs

3.2 Breakthrough curve studies

The starting concentration of solute, bed height, and inflow flow rates are some of the variables that affect the breakthrough curve's distinctive shape (Aksu *et al.* 1998; Gabaldon *et al.* 2000). The equilibrium between the solute and adsorbent, the adsorption rate, and the mechanism of

transfer determine the adsorption capacity of a packed column with given dimensions (Mohamadinejad, Knox and Smith. 2000). The curve's sharpness shows that the mass transfers operation is driving the system's rate process, which is proportionate to that phase's solute content, in addition to displaying an equilibrium isotherm that is linear or non-linear. The current study's curve's form indicates that mass transfer mostly governs adsorption.

3.2.1. Effect of Initial Fluoride Concentration

The breakthrough curve was examined to determine the impact of changing the starting fluoride level, which ranged from 10 to 14 ppm. Other experimental parameters, such as height of the bed (7 cm) and rate of flow (7 mL/min), were maintained constant. The findings are shown in Fig.5. The elimination efficiency was 4.57 % at lower fluoride concntrations and decreased to 3.38 % and 2.57 % at higher concentration (Table 1). This is because when fluoride concentrations grow, fewer adsorption sites will be covered, reducing the percentage of fluoride removal. Because of the smaller concentration gradient caused by a decreased mass transfer coefficient, the saturation time is similarly delayed with lower lower concentrations. The faster saturation of the adsorbent and the mass load on the adsorbent are linked to the faster breakthrough and shorter exhaustion period that occurred as the concentration rose. Cosequently, the concentration influenced the process of adsorption (Das *et al.* 2021; Bacelo *et al.* 2022).

Table 1. Effect of Initial Fluoride Concentration on percentage of adsorption

Initial Fluoride Concentration (ppm)	**Q_{ad}**	**Q_{total}**	**% Removal**
10	980	20650	4.57
12	682.5	20160	3.38
14	542.5	21070	2.57

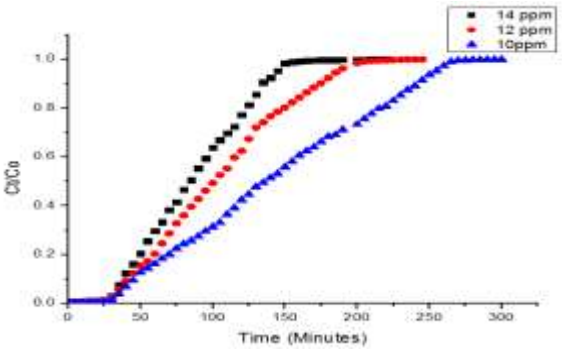

Fig. 5: Effect of Initial fluoride concentration on the breakthrough curve for fluoride adsorption with bed height = 7 cm , flow rate = 7 mL/min

3.2.2 Effect of flow rate

By maintaining height of the bed at 7 cm and the initial concentration of fluoride at 10 ppm while increasing the rate of flow from 7 to 10 mL/min, the breakthrough curve of fluoride biosorption by sunflower seed husk was examined (Table 2). At first, the adsorption occurred extremely quickly at reduced rates of flow, because there were sites of biosorption available for absorbing fluoride inside or surrounding the husk. The uptake becomes less effective in the following step of the process because these sites are gradually occupied. Higher flow rates led to a quicker breakthrough, as shown in Fig.6. The fluoride in the solution could attach to the adsorbent if given enough consistent time (Singh, Kumar and Gaur. 2012). At greater flow rates, fluoride had a shorter residence period. Consequently, exhaustion happened more quickly at high flow rates than at lower flow rates. With increasing flow rates, the breakthrough curves slanted downward (Nur *et al.* 2014; Bishayee *et al.* 2021). The maximum amount of fluoride was removed at a minimum rate of flow (7 ml/min) because the fluoride solution and adsorbent were in touch with one another for a longer duration. The percentage of fluoride removed, as influenced by the incoming flow rate.

Table 2. Effect of Flow rate on percentage of adsorption

Flow rate (mL/min)	**Q_{ad}**	**Q_{total}**	**% Removal**
7	514.5	17500	2.94
8.5	510	17425	2.92
10	580	18000	2.66

3.2.3. Effect of bed height

The performance of fixed-bed columns is significantly impacted by the bed height since it directly affects the adsorbent dosage. The breakthrough curve was examined in relation to bed height (5, 7, and 9 cm) and fixed operating conditions, such as 10 ppm of F^- at the start and 7 mL/min of rate of flow. The elimination of fluoride rose with bed height because the fluoride solution was in contact with the adsorbent for a longer period of time. The fluoride concentration in the wastewater therefore dropped. The mass transfer zone expanded as the bed height grew, as seen in Fig.7, as the breakthrough curve's slope decreased. According to the findings, longer the bed height, longer will be the breakthrough and exhaustion times. This is because there are more binding sites available for sorption. The breakthrough curves become sharper at lower bed heights as the curve's slope rises (Chatterjee, Mondal and De. 2018; Yanyan *et al.* 2018). The higher bed height expanded the mass transfer zone and enhanced the possibilities of contact for catching F^- (Kumari *et al.* 2020). The results of the bed height effect were shown (Table 3).

Table 3. Effect of bed height on percentage of adsorption

Bed height (cm)	Q_{ad}	Q_{total}	% Removal
5	665	16100	4.13
7	770	17500	4.40
9	945	20650	4.57

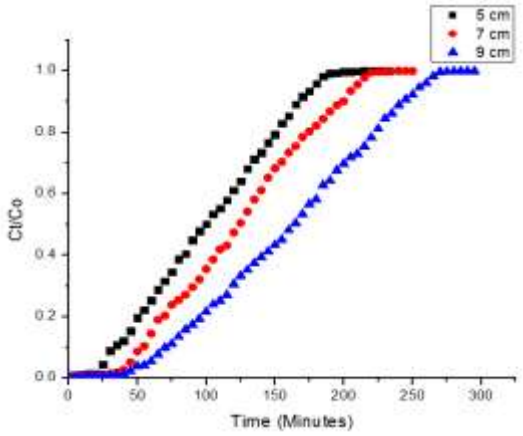

Fig. 7: Effect of Bed height on the breakthrough curve for fluoride adsorption with Initial fluoride concentration = 10 ppm, flow rate = 7 mL/min

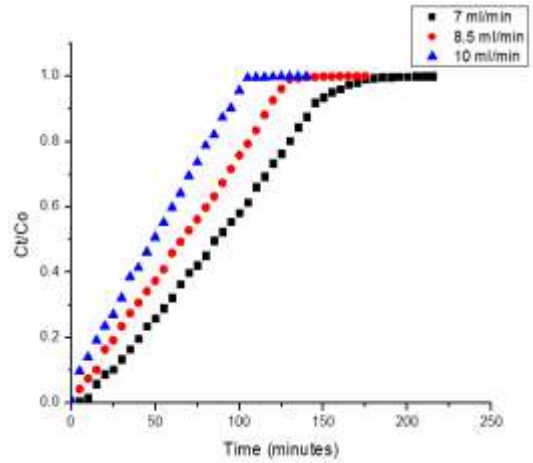

Fig. 6: Effect of flow rate on the breakthrough curve for fluoride adsorption with Bed height = 7 cm, Initial fluoride concentration = 10 ppm

3.3. Columnar adsorption models

Predicting the breakthrough curve of the effluent is crucial for designing an efficient column during the adsorption process. The process of adsorption in columns has been described by a number of mathematical models (Vinodhini and Das, 2010). The column's performance in

adsorbing zirconium-doped sunflower seed husk as an adsorbent was predicted by utilizing the Yoon-Nelson and Thomas models.

3.3.1. Thomas Model

Fluoride ions from a liquid solution are said to be adsorbed onto the adsorbent surface by the model through intra-particle diffusion and sorption at the reaction site (Askari *et al.* 2019). For examining and predicting the behavior of fixed-bed adsorption systems, this model is a useful resource.

The Thomas model is expressed by equation 5:

$$\ln[(\frac{C_o}{C_t}) - 1] = \frac{K_{TH} q_{TH} m}{Q} - K_{TH} C_o t \qquad (5)$$

Where: C_t = amount of effluent at time t, C_o= initial concentration, K_{TH} = rate constant of Thomas model (mL/mg/min), q_{TH} = capacity of maximum adsorption (mg/g), m = adsorbent mass (g), Q = flow rate (L/min).

The experimental data was fitted to the Thomas model equation to get the adsorption capacity (q_{TH}) and the rate constant of Thomas model (K_{TH}), also referred to as the kinetic coefficient. The associated model parameters that were determined from the linear plot shown in Fig.8 (a), (b), and (c) and provides a summary (Table 4). Nearly all correlation coefficients of correlation had strong R^2 values near 1, indicating that the projected value q_{TH} fit the data satisfactorily (Table 4), as seen in Fig.8. Except for the rate of flow of 8.5 and 10 mL/min, which have lower R^2 values of 0.899 and 0.894, R2 values are high for the majority of data points. This implies a possible departure from the presumptions of the Thomas model (Banerjee, Ramesh and Gandhimathi. 2012).

As the initial influent F^- concentration increased, Table 4 showed that the projected value q_{TH} declined. The driving force for adsorption decreased as concentration increased, which led to this outcome (Chen *et al.* 2012). Because of insufficient time spent in contact between the adsorbent and F^-, the expected value q_{TH} decreased as the inflow rate increased. As the height of the bed increased, the q_{TH} value decreased because higher bed heights have fewer active sites (Castel *et al.* 2000). As bed height increased, the opposition between the solid and liquid states increased, lowering the rate of mass transfer and causing the K_{TH} values to decrease (Du, Zheng and Wang. 2018). The higher the initial fluoride content, the lower the K_{TH} value. This resulted from an increase in the driving force for adsorption with concentration. Since fluoride's residence time in the bed was extremely high in this instance, K_{TH} grew as the rate of flow rose.

Table 4. Thomas model constants for different factors investigated for column studies

Column Kinetic models	**Flow rates (mL/min)**			**Bed Height (cm)**			**Initial concentration (ppm)**		
	7	**8.5**	**10**	**5**	**7**	**9**	**14**	**12**	**10**
K_{TH} (mL/mg/min)	0.0051	0.0063	0.0073	0.0045	0.0042	0.0034	0.0033	0.0038	0.0042
q_{TH}	0.91	0.909	0.909	0.98	0.92	0.90	0.90	1.09	1.27
R^2	0.92	0.899	0.894	0.92	0.90	0.91	0.90	0.95	0.97

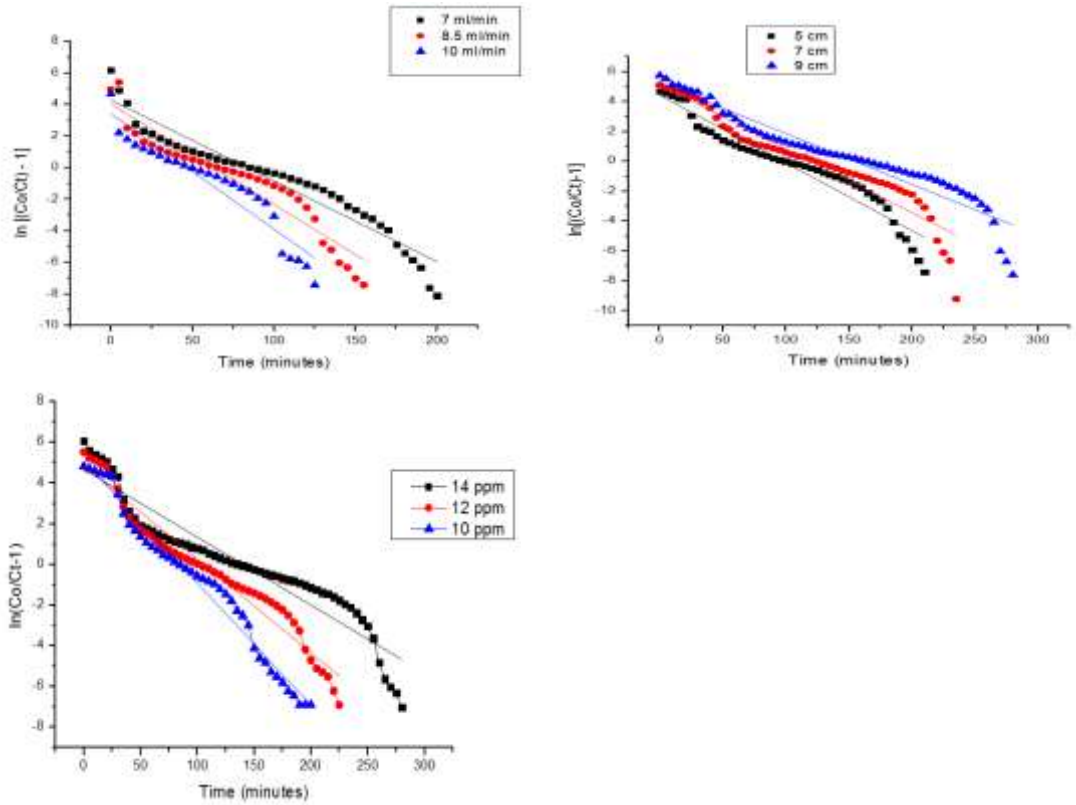

Fig. 8: Plot of breakthrough curves of Thomas model for fluoride removal at different (a) Flow rates, (b) Bed heights and (c) Initial fluoride concentrations

3.3.2. Yoon-Nelson Model

This model assumes that the adsorption of adsorbate and the chance of breakthrough are directly correlated with the adsorption probability of each adsorbate molecule. It is frequently used to calculate the amount of time required for a 50% breakthrough in pollutants (Gupta and Garg, 2019). Yoon-Nelson model could be presented as Equation 6.

$$\ln\left[\frac{C_t}{C_o - C_t}\right] = K_{YN}t - K_{YN}\tau \qquad (6)$$

Where: C_t = effluent concentration at time t, C_0 = initial concentration, K_{YN} (min^{-1}) and τ (min) denoted the Yoon-Nelson rate constant and τ (min) denoted the time needed for a 50% F^- breakthrough, and t is the sampling time.

The values of τ and K_{YN} that were determined by modeling the experimental results to the Yoon-Nelson equation (Table 5) and Fig.9 (a), (b), (c) provides a summary of the related model parameters identified from the linear plot.

Plots with high R2 values near 1 showed that the Yoon-Nelson model and experimental data fit each other well under various experimental settings. Most of the data points have high R^2 values, except for the flow rates of 8.5 mL/min and 10 ml/min which has lower R^2 of 0.899 and 0.894 respectively. This suggests a potential deviation from Yoon-Nelson model assumptions.

The K_{YN} values increased as the inflow rate increased (Table 5). This suggests that while the adsorption rate increases with greater flow rates, it takes less time for the effluent concentration to reach 50% of the influent concentration. It will take less time to achieve the 50% breakthrough point since the drop in τ with flow rate indicates that fewer adsorbate molecules are being processed per unit of time (Bai *et al.* 2018). As the influent concentration increases K_{YN} decreases due to decreased driving force for adsorption. The rise in τ suggests that additional time is required to achieve the 50% breakthrough. As the bed height increases, K_{YN} decreases,the τ value increases. More contact time and surface area for adsorption are provided by a higher bed height, which leads to a lower adsorption rate constant KYN and a longer time to 50% breakthrough. Accordingly, by reducing the number of adsorption sites, raising the bed height can improve adsorption effectiveness.

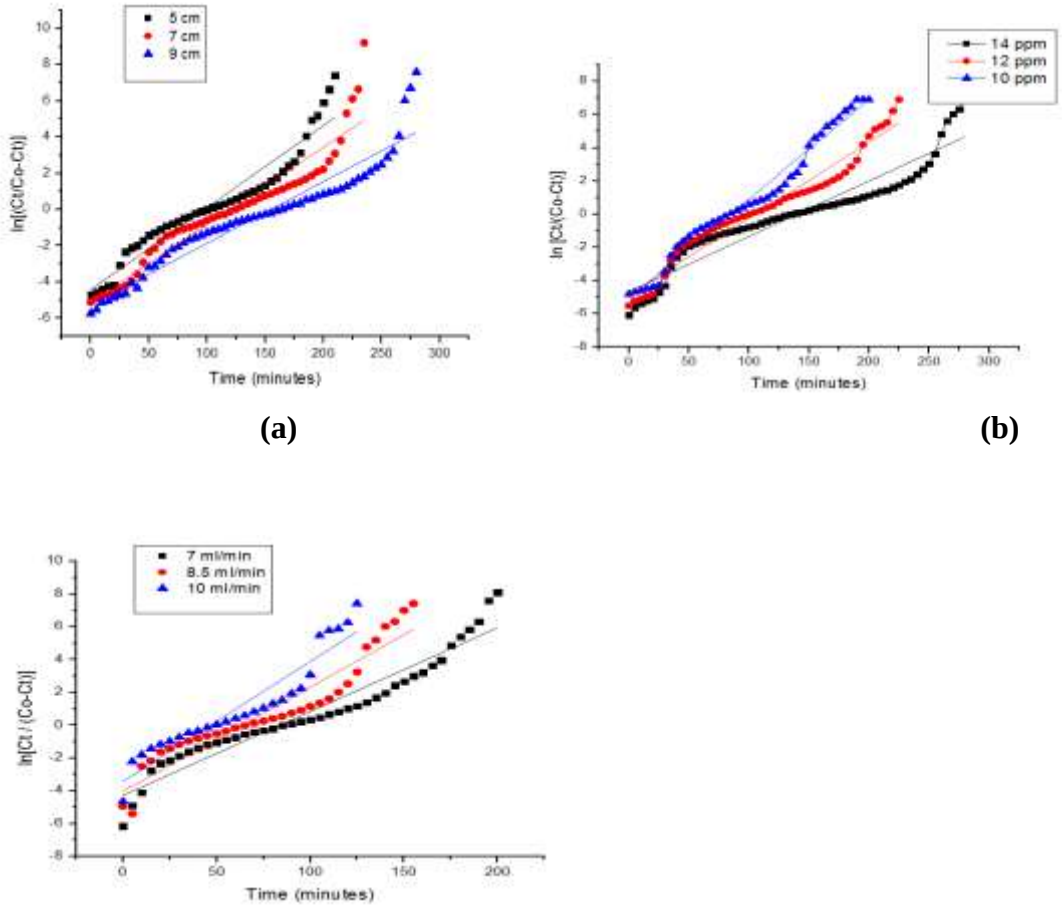

(a) **(b)**

(c)

Fig. 9: Plot of breakthrough curves of Yoon-Nelson model for fluoride removal at different (a) Flow rates, (b) Bed heights and (c) Initial fluoride concentrations

Table 5. Yoon-Nelson model constants for different factors investigated for column studies

Column Kinetic models	Flow rates (mL/min)			Bed Height (cm)			Initial concentration (ppm)		
	7	8.5	10	5	7	9	14	12	10
K_{YN} (L/min)	0.051	0.055	0.073	0.045	0.042	0.034	0.033	0.046	0.059
τ (min)	83.65	63.32	46.69	97.61	119.62	154.67	138.81	105.80	84.94
R^2	0.92	0.899	0.894	0.92	0.90	0.91	0.90	0.95	0.97

3.4. Desorption, regeneration and reuse studies

Regeneration of the adsorbent is necessary for the adsorption process to be suitable for large-scale use. An appropriate eluent solution can desorb fluoride that has been adsorbed on the adsorbent, permitting its application in several cycles of adsorption and desorption. At a rate of flow of 7 mL/min, the zirconium-activated carbon adsorbent was renewed using 0.1 M HCl. The column was designed to allow the desorbing fluid to pass through it. Fluoride levels in the effluent were measured on a regular basis. After the effluent fluoride concentration dropped to zero, the desorbing solution's flow was halted. The column was then filled with distilled water until the effluent's pH approached 7. Four trials using the regeneration approach were conducted in the same experiment. As the number of cycles rose, the exhaustion time gradually decreased due to the bed's regeneration (Jamwal and Slathia, 2022). Fig.10 displays the findings of the reuse investigations, which were conducted up to four reuse cycles. The first reuse showed 27.69%, the removal efficiency decreased as the number of reuses grew, and in the fourth cycle, the removal efficiency was 23.07% (Table 6). Continuous use may cause zirconium oxide's structural integrity to get distracted, which would lower the fluoride removal efficiency.

Table 6. Regeneration studies for different factors investigated for column studies

Number of cycles	Q_{ad}	Q_{total}	% Removal
1	2520	9100	27.69
2	1890	7700	24.54
3	1295	5600	23.12
4	1050	4550	23.07

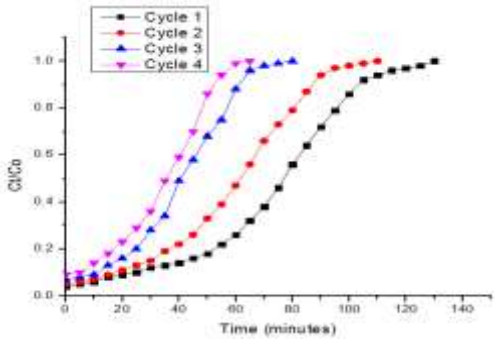

Fig. 10: (a) Regeneration studies graphs for optimum bed height (9 cm), initial fluoride concentration (10 ppm) and flow rate (7 ml/min)

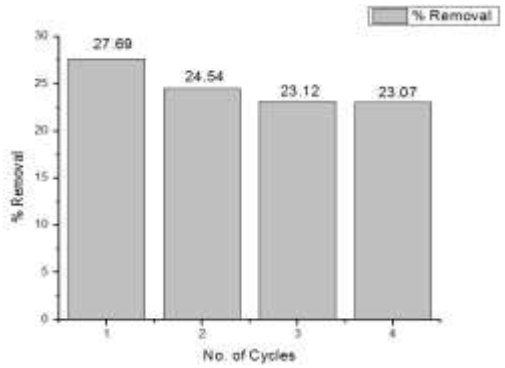

Fig. 10: (b) Reusability studies for four different cycles

3.5. Case Study

The column arrangement designed for fluoride removal with ZrO_2/SSH as adsorbent was used to treat samples gathered from several locations within the Tumakuru district's Pavagada taluk, Karnataka state, India. Sample 1 was obtained from Venkatapura village (Panchayathi bore) and sample 2 was collected from Pavagada rural (Subbarayappa borewell). To find out if the adsorbent was suitable for eliminating fluoride, experiments were conducted utilizing 40 g of the substance. Water polluted with fluoride was moved upward across the column at a speed of 7 mL/min. A 100 ml sample of treated water was taken from each batch and examined separately. Water analysis was conducted to understand the effects of different ions present in the actual field water samples by testing and comparing them with the standard drinking water limits (Table 7). Thus, the case study indicates that the synthesized adsorbent was able to remove fluoride as well as other contaminants.

Table 7. Values of treated and untreated water collected from the Pavagada district of Karnataka

Source	**Venkatapura (Panchayathi Borewell)**		**Pavagada Rural (Subbarayappa Beorewell)**		**Permissible Limit**
Parameters	**Influent water**	**Treated water**	**Influent water**	**Treated water**	
Ph	7.18	6.8	7.2	7.0	6.5-8.5
Conductance (µS/cm)	1.0	0.9	1.4	1.1	0.5-3
Sulfate (mg/L)	148	68	170	110	200-400
Nitrate (mg/L)	0.9	0.6	1.5	1.2	45
COD (mg/L)	764	380	772	390	250
Total Hardness(mg/L)	848	386	984	531	300-600
Calcium Hardness	148	86	184	116	75-200

Magnesium Hardness (mg/L)	700	300	800	415	30-100
Alkalinity (mg/L)	520	320	540	350	200-600
Chloride (mg/L)	1159.3	869	1186	870	250-1000
Acidity (mg/L)	56	44	57	46	15-400
DO (mg/L)	27.58	20.89	29.7	23.65	6.5-8
BOD (mg/L)	8	5	9	6	1-5
Fluoride (mg/L)	1.9	1.011	2.47	1.036	1-1.5

4. CONCLUSION

The breakthrough curves showed a maximum adsorption of 2.94% for the minimum flow rate, 4.51% for the minimum fluoride concentration, and 4.51% for the highest bed height. Raising the rate of flow from 7 to 10 mL/min results in a little increase in q_{TH}, whereas R2 values are above 0.96 or around 1. As the concentration of fluoride ion increases from 10 to 14 mg/L, the data shows a significant increase in q_{TH}. This implies a greater capacity for adsorption at elevated concentrations. The adsorbent can be reused with satisfactory removal efficiency (up to 23.07 percent removal on the fourth cycle), according to the reuse experiments, and the fluoride ion can be efficiently desorbed. The effectiveness of zirconium-doped sunflower seed shells for real-world uses is demonstrated by the Thomas and Yoon-Nelson models. According to this work, zirconium-doped sunflower seed husk is a natural, eco-friendly, economical, and promising fluoride adsorbent from aqueous solutions.

ACKNOWLEDGMENTS

Author, BNS thank the Principal, Sri Siddhartha Academy of Higher Education, Agalkote, Tumkur, Karnataka, India for providing research facilities. HVJ and HSL also thank the Principal, CEO and Director of Siddaganga Institute of Technology, Tumakuru, Karnataka for the research facilities.

FUNDING

No specific grant from a public, private, or nonprofit organization was obtained for this study.

CONFLICTS OF INTEREST

There is no conflict of interest, according to the authors.

REFERENCES

Annu, A., Sivasankari, C. and Krupasankar, U., Synthesis and characerization of ZrO_2 nanoparticle by leaf extract bioreduction process for its biological studies, *Materials Today: Proceedings*, 33, 5317-5323,(2020). https://doi.org/10.1016/j.matpr.2020.02.975

Aksu, Z., Ãzer, D., Ãzer, A., Kutsal, T. and Çaglar, A., Investigation of the Column Performance of Cadmium(II) Biosorption by Cladophora crispata Flocs in a Packed Bed, *Separation Science and Technology*, 33(5), 667-682 (1998). https://doi.org/10.1080/01496399808544782

Aksu, Z. and Gönen, F., Biosorption of phenol by immobilized activated sludge in a continuous packed bed: prediction of breakthrough curves, *Process Biochemistry*. 39(5), 599-613 (2004). https://doi.org/10.1016/S0032-9592(03)00132-8

Al-Zaqri, N., Muthuvel, A., Jothibas, M., Alsalme, A., Alharthi, F. A. and Mohana, V., Biosynthesis of zirconium oxide nanoparticles using Wrightia tinctoria leaf extract: characterization, photocatalytic degradation and antibacterial activities, *Inorganic Chemistry Communications*, 127, 108507, (2021). https://doi.org/10.1016/j.inoche.2021.108507.

Askari, M., Salehi, E., Ebrahimi, M. and Barati, A., Application of breakthrough curve analysis and response surface methodology for optimization of a hybrid separation system consisting of fixed-bed column adsorption and dead-end depth filtration, *Chemical Engineering and Processing – Process Intensification*, 143, 107594 (2019).https://doi.org/10.1016/j.cep.2019.107594

Asuquo, E. D., Martin, A. D. and Nzerem, P., Evaluation of Cd (II) ion removal from aqueous solution by a low-cost adsorbent prepared from white yam (Dioscorea rotundata) waste using batch sorption, *Chem Engineering*, 2(3), 35-71 (2018). https://doi.org/10.3390/chemengineering2030035.

Bacelo, H., Santos, S. C., Ribeiro, A., Boaventura, R. A. and Botelho, C. M., Antimony removal from water by pine bark tannin resin: Batch and fixed-bed adsorption, *J. Environ. Manag*, 302, 114100 (2022). https://doi.org/10.1016/j.jenvman.2021.114100

Bai, B., Xu, X., Li, C., Xing, J., Wang, H. and Suo, Y., Magnetic Fe_3O_4@Chitosan Carbon Microbeads: Removal of Doxycycline from Aqueous Solutions through a Fixed Bed via Sequential Adsorption and Heterogeneous Fenton-Like Regeneration, *J. Nanomater*, 2018(1), 5296410 (2018). https://doi.org/10.1155/2018/5296410.

Bai, S., Li, J., Ding, W., Chen, S. and Ya, R., Removal of boron by a modified resin in fixed bed column: Breakthrough curve analysis using dynamic adsorption models and artificial neural network model, *Chemosphere*, 296, 134021 (2022). https://doi.org/10.1016/j.chemosphere.20

Banerjee, K., Ramesh, S.T. and Gandhimathi, R., A novel agricultural waste adsorbent, watermelon shell for the removal of copper from aqueous solutions, *Iran. J. Energy Environ*, 3(2), 143–156 (2012). https://doi.org/10.5829/idosi.ijee.2012.03.02.0396.22.134021.

Bishayee, B., Ruj, B., Nandi, S., Chatterjee, R. P., Mallick, A., Chakraborty, P., Nayak, J. and Chakrabortty, S., Sorptive elimination of fluoride from contaminated groundwater in a fixed bed column: A kinetic model validation based study, *J. Indian Chem. Soc*, 99(1), 100302 (2021). https://doi.org/10.1016/j.jics.2021.100302.

Castel, C., Schweizer, M., Simomonnot, M. O. and Sardin, M., Selective removal of fluoride ions by a two-way- ion –exchange cyclic process, *Chemical Engineering Science*, 55(17), 3341-3352 (2000). https://doi.org/10.1016/S0009-2509(00)00009-9.

Chatterjee, S, Mondal, S. and De, S., Design and scaling up of fixed bed adsorption columns for lead removal by treated laterite, *J. Clean. Prod*, 177, 760–774 (2018).https://doi.org/10.1016/j.jclepro.2017.12.249.

Chen, S., Yue, Q., Gao, B., Li, Q., Xu, X. and Fu, K., Adsorption of hexavalent chromium from aqueous solution by modified corn stalk: A fixed-bed column study, *Bioresour. Technol*, 113, 114–120 (2012). https://doi.org/10.1016/j.biortech.2011.11.110.

Das, L., Sengupta, S., Das, P., Bhowal, A. and Bhattacharjee, C., Experimental and Numerical modeling on dye adsorption using pyrolyzed mesoporous biochar in Batch and fixed-bed column reactor: Isotherm, Thermodynamics, Mass transfer, Kinetic analysis, *Surf. Interfaces*, 23, 100985 (2021). https://doi.org/10.1016/j.surfin.2021.100985.

Du, Z., Zheng, T. and Wang, P., Experimental and modelling studies on fixed bed adsorption for Cu(II) removal from aqueous solution by carboxyl modified jute fiber, *Powder Technol*, 338, 952–959(2018). https://doi.org/10.1016/j.powtec.2018.06.015.

Feizi, M. and Jalali, M., Removal of heavy metals from aqueous solutions using sunflower, potato, canola and walnut shell residues, *J. Taiwan Inst. Chem. Eng*, 54,125-136(2015). https://doi.org/10.1016/j.jtice.2015.03.027.

Gabaldon, C., Marzal, P., Seco, A. and Gonzalez, J. A., Cadmium and Copper Removal by a Granular Activated Carbon in Laboratory Column Systems, *Separation Science and Technology*, 35(7), 1039-1053 (2000). https://doi.org/10.1081/SS-100100209

Goyal, P., Bhardwaj, A., Mehta, B. K. and Mehta, D., Research article green synthesis of zirconium oxide nanoparticles (ZrO_2NPs) using Helianthus annuus seed and their antimicrobial effects, Journal of the Indian Chemical Society, 98(8), 100089, (2021). https://doi.org/10.1016/j.jics.2021.100089

Gupta, A. and Garg, A., Adsorption and oxidation of ciprofloxacin in a fixed bed column using activated sludge derived activated carbon, *J. Environ. Manag*, 250,109474(2019). https://doi.org/10.1016/j.jenvman.2019.109474

Hiremath, P. G. and Theodore, T., Biosorption of fluoride from synthetic and ground water using Chlorella vulgaris immobilized in calcium alginate beads in an upflow packed bed column, *Periodica Polytechnica Chemical Engineering*, 61(3), 188-199 (2017). https://doi.org/10.3311/PPch.10085

Jain, M., Garg, V. K. and Kadirvelu, K., Chromium (VI) removal from aqueous system using Helianthus annuus (sunflower) stem waste, *J. Hazard. Mater*, 162(1),365-372(2009). https://doi.org/10.1016/j.jhazmat.2008.05.048.

Jamwal, K. D. and Slathia, D. A., Review of Defluoridation Techniques of Global and Indian Prominence, *Current World Environment*,17(1), 41-57 (2022). http://dx.doi.org/10.12944/CWE.17.1.5.

Kovo, A. S., Alaya-Ibrahim, S., Abdulkareem, A. S., Adeniyi, O. D., Egbosiuba, T. C., Tijani, J. O., Saheed, M., Okafor, B. O. and Yusuff, A. S., Column adsorption of biological oxygen demand, chemical oxygen demand and total organic carbon from wastewater by magnetite nanoparticles-zeolite. A composite, *Heliyon*, 9(2), 13095-13115 (2023). https://doi.org/10.1016/j.heliyon.2023.e13095.

Kumari, U., Mishra, A., Siddiqi, H. and Meikap, B., Effective defluoridation of industrial wastewater by using acid modified alumina in fixed-bed adsorption column: Experimental and breakthrough curves analysis, *J. Clean. Prod* , 279, 123645 (2020). https://doi.org/10.1016/j.jclepro.2020.123645.

Mani, S. K. and Bhandari, R., Efficient fluoride removal by a fixed-bed column of self-assembled Zr (IV)-, Fe (III)-, Cu (II)- complexed polyvinyl alcohol hydrogel beads, *ACS omega*, 7(17),15048-15063(2022). https://doi.org/10.1021/acsomega.2c00834

Mohamadinejad, H., Knox, J. C. and Smith, J. E., Experimental and Numerical Investigation of Adsorption/Desorption in Packed Sorption Beds under Ideal and Nonideal Flows, *Separation Science and Technology*, 35(1), 1-22 (2000). https://doi.org/10.1081/SS-100100140

Muthuvel, A., Jothibas, M., Manoharan, C. and Jayakumar, S. J., Synthesis of CeO 2-NPs by chemical and biological methods and their photocatalytic, antibacterial and in vitro antioxidant activity, *Research on Chemical Intermediates*, 46, 2705-2729, (2020). https://doi.org/10.1007/s11164-020-04115-w

Nur, T., Loganathan, P., Nguyen, T., Vigneswaran, S., Singh, G. and Kandasamy, J., Batch and column adsorption and desorption of fluoride using hydrous ferric oxide: Solution chemistry and modeling, *Chem. Eng. J*, 247, 93–102 (2014). https://doi.org/10.1016/j.cej.2014.03.009.

Reddy, N. A., Lakshmipathy, R. and Sarada, N. C., Application of Citrullus lanatus rind as biosorbent for removal of trivalent chromium from aqueous solution, *Alex Eng J*, 53(4), 969-975 (2014). https://doi.org/10.1016/j.aej.2014.07.006

Saleh, M. E., El-Refaey, A. A. and Mahmoud, A. H., Effectiveness of Sunflower Seed Husk Biochar for Removing Copper Ions from Wastewater: a Comparative Study, *Soil Water Res*, 11(1), 53–63 (2016). https://doi.org/10.17221/274/2014-SWR

Shinde, H., Bhosale, T., Gavade, N., Babar, S., Kamble, R., Shirke, B. and Garadkar, K., Biosynthesis of ZrO 2 nanoparticles from Ficus benghalensis leaf extract for photocatalytic activity, *Journal of Materials Science: Materials in Electronics*, 29, 14055-14064, (2018). https://doi.org/10.1007/s10854-018-9537-7 .

Singh, A., Kumar, D. and Gaur, J. P., Continuous metal removal from solution and industrial effluents using Spirogyra biomass-packed column reactor, *Water Res*, 46(3), 779–788 (2012). https://doi.org/10.1016/j.watres.2011.11.050.

Suriyaraj, S. P., Ramadoss, G., Chandraraj, K. and Selvakumar, R., One pot facile green synthesis of crystalline bio-ZrO2 nanoparticles using Acinetobacter sp. KCSI1 under room temperature, Materials Science and Engineering: C, 105, 110021, (2019). https://doi.org/10.1016/j.msec.2019.110021

Vinodhini, V. and Das, N., Packed bed column studies on Cr (VI) removal from tannery wastewater by neem sawdust, *Desalination*, 264(1-2), 9-14 (2010). https://doi.org/10.1016/j.desal.2010.06.073

Wang, Q., Chen, P., Zeng, X., Jiang, H., Meng, F., Li, X., Wang, T., Zeng, G., Liu, L., Shu, H. and Luo, X., Synthesis of (ZrO2-Al2O3)/GO nanocomposite by sonochemical method and the mechanism analysis of its high defluoridation, *Journal of hazardous materials*, 381,120954 (2020). https://doi.org/10.1016/j.jhazmat.2019.120954.

Yanyan, L., Kurniawan, T. A., Zhu, M., Ouyang, T., Avtar, R., Othman, M. H. D., Mohammad, B.T. and Albadarin, A. B., Removal of acetaminophen from synthetic wastewater in a fixed-bed column adsorption using low-cost coconut shell waste pretreated with NaOH, HNO_3, ozone, and/or chitosan, *J. Environ. Manag*, 226, 365–376 (2018). https://doi.org/10.1016/j.jenvman.2018.08.032.